ACS OMEGA

http://pubs.acs.org/journal/acsodf

Article

Theoretical Study of NO Dissociative Adsorption onto 3d Metal Particles M_{55} (M = Fe, Co, Ni, and Cu): Relation between the Reactivity and Position of the Metal Element in the Periodic Table

Nozomi Takagi, Masahiro Ehara, and Shigeyoshi Sakaki*

Cite This: *ACS Omega* 2021, 6, 4888−4898

Read Online

ABSTRACT: NO dissociative adsorption onto 3d metal particles M_{55} (M = Fe, Co, Ni, and Cu) was investigated theoretically using density functional theory computations. A transition state exists at higher energy in the Cu case but at lower energy in the Fe, Co, and Ni cases than the reactant (sum of M_{55} and NO), indicating that Cu_{55} is not reactive for NO dissociative adsorption because NO desorption occurs more easily than the N−O bond cleavage in this case, but Fe_{55}, Co_{55}, and Ni_{55} are reactive because NO desorption needs a larger destabilization energy than the N−O bond cleavage. This result agrees with the experimental findings. The energy of transition state E(TS) becomes higher in the order of Fe < Co < Ni ≪ Cu. Exothermicity E_{exo} (relative energy to the reactant) decreases in the order of Fe > Co > Ni ≫ Cu. These results indicate that the reactivity for NO dissociative adsorption decreases kinetically and thermodynamically in this order. In addition, the E(TS) and E_{exo} values show that 3d metal particles are more reactive than 4d metal particles when a comparison is made in the same group of the periodic table. Charge transfer (CT) from the metal particle to NO increases as the reaction proceeds. The CT quantity to NO at the TS increases in the order of Cu < Ni < Co < Fe, identical to the increasing order of reactivity. The negative charges of the N and O atoms of the product (N and O adsorbed M_{55}) increase in the order of Ni < Co < Cu < Fe, identical to the increasing order of E_{exo} except for the Cu case; in the Cu case, the discrepancy between the order of E_{exo} and those of the N and O negative charges arises from the presence of valence 4s electron of Cu because it suppresses the CT from N and O to Cu_{55}. From these results, one can infer that the d-valence band-top energy of M_{55} plays an important role in determining the reactivity for NO dissociative adsorption. Truly, the d valence orbital energy decreases in the order of Fe > Co > Ni ≫ Cu and the 3d metal > 4d metal in the same group of the periodic table, which reflects the dependence of reactivity on the metal element position in the periodic table.

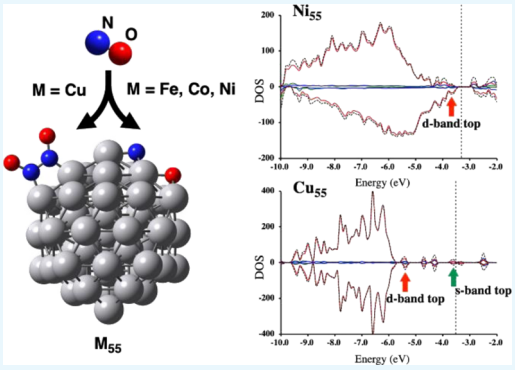

■ INTRODUCTION

The reduction of nitrogen monoxide, NO, to N_2 is one of the important reactions in a three-way catalyst (TWC) for cleaning automobile exhaust gas, as is well known.[1−6] Rh metal particles have been used as one of the key components of TWC for NO reduction for a long time.[7−10] However, the rhodium resources on the earth are extremely limited. As the dissociative adsorption of NO onto Rh metal particles is believed to be the first step of NO reduction, it is crucially important to understand whether and how NO dissociative adsorption occurs on various metals, in particular, on cheap and abundant 3d transition metals.

Many reports of the relevant literature have described experiments elucidating NO reaction behavior on metal particles and surfaces.[11−15] Summarizing those reports, the reaction behavior of the NO molecule on metal particles and surfaces can be classified into three categories, (i) NO dissociative adsorption with the N−O bond cleavage, (ii) NO molecular adsorption without the N−O bond cleavage, and (iii) NO dimerization through N−N bond formation. It is particularly interesting that the NO reaction behavior depends on the metal element position in the periodic table.[12] For instance, NO dissociative adsorption was reported to occur on group VI (Mo and W), VII (Re), VIII (Fe and Ru), and IX (Co, Rh, and Ir) metal surfaces at room temperature and even at lower temperatures.[12] In the case of group X metal elements, however, NO dissociative adsorption was reported to occur on the Ni metal surface, but NO molecular adsorption was reported on Pd and Pt metal surfaces. In the case of group XI metal elements, NO dimerization was reported to occur on Cu[16,17] and Ag metal surfaces,[18,19] whereas the Au metal

Received: December 1, 2020
Accepted: January 29, 2021
Published: February 10, 2021

https://dx.doi.org/10.1021/acsomega.0c05838
ACS Omega 2021, 6, 4888−4898

surface is expected to be inert for NO dimerization and to undergo only NO molecular adsorption.[12]

Differences in the reactivities of metal elements for NO dissociative adsorption were discussed in terms of the melting point of bulk metals, as follows:[12] when the d-shell is half occupied, metal−metal bonds are the strongest. Therefore, the cohesive energy is large and the melting point is high. Such metal particles and surfaces can form strong M−N and M−O bonds because the half-occupied d-shell contributes well to the M−N and M−O bonds. Therefore, the melting point is related to the reactivity for NO dissociative adsorption. Nevertheless, this understanding is not perfect. For instance, the Pd metal melting point is slightly higher than those of Fe, Co, and Ni, whereas the Pd metal is not reactive for NO dissociative adsorption but Fe, Co, and Ni metals are reactive, as described above. Such phenomena lead us to pose one important open question: Do more general properties of metal elements explain the NO dissociative adsorption reactivity?

Another noteworthy point is that the reactivity of Ni for NO dissociative adsorption differs greatly from those of Pd and Pt, although these elements belong to the same group X. Regarding group IX elements, however, Co, Rh, and Ir are all reactive for NO dissociative adsorption.[12] These results present us with a second open question: Why does Ni differ so much from Pd and Pt for NO dissociative adsorption in group X, whereas Co exhibits similar reactivity to those of Rh and Ir in group IX?

To obtain correct answers to the questions presented above, one must perform theoretical studies of NO dissociative adsorption onto metal particles and surfaces. NO molecular adsorption has been investigated theoretically many times.[20−36] Nevertheless, theoretical studies of NO dissociative adsorption onto metal particles and surfaces have been limited except for a few works. For instance, NO dissociative adsorption onto Rh metal particles and Rh(111) surface has been investigated theoretically by Nakai and co-workers.[37] In addition, a first-principles microkinetic study of NO dissociative adsorption and NO−CO reaction on the Rh(111) surface has been reported by Ishikawa and Tateyama.[38] Recently, NO dissociative adsorption and NO dimerization on M_{55} and M_{13} (M = Ru, Rh, Pd, and Ag) have been investigated theoretically.[39,40] In the case of 3d metals, NO dissociative adsorption onto Cu_{13} and Cu_{38} has been discussed in recent theoretical works,[41,42] but no systematic theoretical study of NO dissociative adsorption onto other 3d metal particles and surfaces has been reported yet. Consequently, a systematic theoretical study of NO dissociative adsorption onto 3d metal particles is necessary for obtaining theoretical answers to the open questions posed above and for understanding the differences and similarities in reactivity for NO dissociative adsorption between 3d and 4d metal particles.

For this work, we theoretically investigated NO dissociative adsorption onto 3d metal particles such as Fe_{55}, Co_{55}, Ni_{55}, and Cu_{55}, where the icosahedral structure (Scheme 1) was used; the section "Computational Details and Models" below presents the reason. Our purposes here are (i) to explore the reactivity of these metal particles for NO dissociative adsorption, (ii) to compare the reactivity for NO dissociative adsorption between 3d and 4d metals, in particular, between Ni and Pd (group X) and between Co and Rh (group IX), (iii) to ascertain what property of metal particle determines the reactivity for NO dissociative adsorption, and (iv) to elucidate the relation between the metal particle reactivity for NO dissociative adsorption and the metal element position in the periodic table based on the metal particle electronic structure. Although NO dissociative adsorption onto Cu clusters has been investigated theoretically using Cu_{13} and Cu_{38},[41,42] we re-investigated NO dissociative adsorption onto Cu_{55} for a better comparison with Ag_{55}, which was employed as a model in a theoretical study of NO reactions on 4d metal particles.[39] Throughout this work, we intended to present general knowledge of the relation between the electronic structure of the metal particle and reactivity for NO dissociative adsorption.

Scheme 1. Icosahedral Structure of the M_{55} Particle (M = Fe, Co, Ni, or Cu) Investigated Here (a) and Edge and Vertex Positions on the Surface (b)

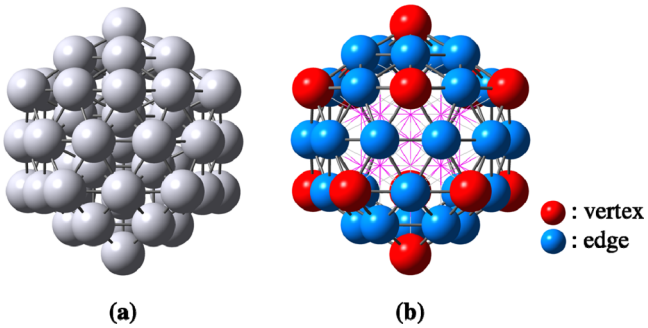

■ RESULTS AND DISCUSSION

Geometry Changes in NO Dissociative Adsorption onto Fe_{55}, Co_{55}, Ni_{55}, and Cu_{55}. NO is adsorbed onto M_{55} at both the vertex and edge sites, where the adsorption at the vertex site is moderately more stable than at the edge site. Table S1 of the Supporting Information presents a comparison of these two adsorption sites. As shown in Figure 1, NO adsorption at the vertex site occurs through the N atom in an end-on adsorption manner in all these 3d M_{55} particles like that in 4d M_{55} particles (M = Ru, Rh, Pd, and Ag).[39] This adsorption species is designated as **1**; the extent of spin polarization is presented in Table S2 of the Supporting Information. NO has an almost linear adsorption structure (M−N−O angle = 179−180°) in the Fe and Co cases and a slightly bending structure (175°) in the Ni case, whereas NO is adsorbed onto Cu_{55} in a somewhat bending structure (M−N−O angle = 161°). The reason for this difference is discussed in the section below. The M−N distance is 1.63−1.64 Å in Fe_{55}, Co_{55}, and Ni_{55}, but somewhat longer in Cu_{55} by 0.12 Å, which is consistent with the lower adsorption energy in the Cu case, as discussed below. The N−O distance is moderately longer than that of a free NO molecule (1.172 Å), but it does not differ much among these metal particles. The NO stretching frequency is a useful property for investigating the interaction of the NO molecule with the metal surface, but its computed value does not agree well with the experimentally obtained value.[12] The disagreement is not unreasonable because M_{55} was used for the calculations, but the bulk metal surface was used for experimental measurements; Table S3 of the Supporting Information presents a comparison.

The N−O bond cleavage is likely to occur starting from the NO side-on adsorption structure. Therefore, we investigated the side-on adsorption structure **2** (Figure 1). The N−O distance is somewhat elongated in Fe_{55} and Co_{55} but only moderately so in Ni_{55} and Cu_{55}. The M−N distance is shorter

https://dx.doi.org/10.1021/acsomega.0c05838
ACS Omega 2021, 6, 4888−4898

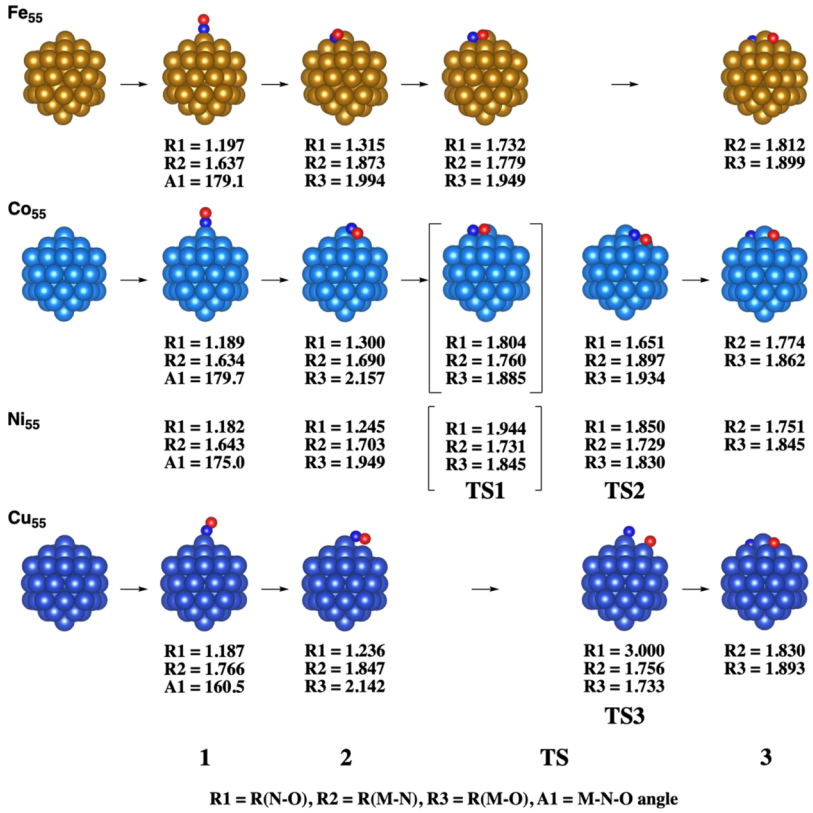

Figure 1. Geometry changes in N−O dissociative adsorption onto Fe_{55}, Co_{55}, Ni_{55}, and Cu_{55}. Distances are in angstrom. In Ni_{55} and Co_{55}, transition states of two kinds were located, whereas in Fe_{55} and Cu_{55}, only one transition state was located. *R*1, *R*2, *R*3, and *A*1, respectively, represent the N−O, M−N, and M−O distances (in angstrom) and M−N−O angle (in degree). *R*2 and *R*3 are the averaged values of M−N and M−O distances because N and O atoms exist at the bridge or hollow site in **2**, **TS**, and **3**.

than the M−O distance in all these intermediates. Then, the N−O bond is cleaved via a transition state to afford an N, O-adsorbed species **3** in which N and O atoms exist at the hollow site of the surface. In the reaction on Fe_{55}, only one transition state (**TS1**) was located, whereas in the Co_{55} and Ni_{55} cases, transition states of two kinds, **TS1** and **TS2**, were located. In **TS1**, each of the N and O atoms exists at a bridging position between the vertex and edge M atoms. In **TS2**, the N atom exists at a hollow position of vertex and two edge M atoms, but the O atom exists at a bridging position between the vertex and edge M atoms. In the reaction on Cu_{55}, only one **TS3** was located. In this **TS3**, the N and O atoms exist, respectively, at atop positions of vertex and edge Cu atoms. At all these **TS**s, the N−O distance is elongated considerably; it lengthens in the order of $Fe_{55} < Co_{55} < Ni_{55}$ in **TS1**. However, the N−O distance at **TS2** is somewhat shorter than that at **TS1** in the Co and Ni cases, indicating that the character of **TS2** differs from that of **TS1**. **TS3** of the Cu case is more product-like than either **TS1** or **TS2** of the Co and Ni cases because the N−O bond is longer in **TS3** than in either **TS1** or **TS2**. This geometrical feature of **TS3** suggests that NO dissociative adsorption is difficult in the Cu case, as discussed below. In product **3**, the M−N and M−O distances lengthen in the order of $Ni_{55} < Co_{55} < Fe_{55} \ll Cu_{55}$. This order does not fit the decreasing order of reaction energy, as discussed below, but this order seems reasonable because the 3d atomic orbital becomes larger as Ni < Co < Fe.[43,44] In the case of Cu, the much larger 4s orbital participates in these bonds.[43,44]

It is noteworthy here that the N−O distance at TS is somewhat shorter in the 3d metal case than in the 4d metal case; 1.744 Å for Ru_{55}, 1.982 Å for Rh_{55}, 2.764 Å for Pd_{55}, and 3.137 Å for Ag_{55}.[39] This difference between 3d and 4d metals suggests that the NO dissociative adsorption onto the 3d metal particle occurs through an earlier (more reactant-like) transition state than that onto the 4d metal particle, which is expected to be related to the differences in reactivity between 3d and 4d metal particles, the discussion of which is presented below.

Energy Changes in NO Dissociative Adsorption onto Fe_{55}, Co_{55}, Ni_{55}, and Cu_{55}. In this section, we mainly used potential energy without zero-point energy correction for discussion because the Gibbs energy and frequencies were evaluated approximately here, as described below in the section "Computational Details and Models". Only for the discussion of NO adsorption/desorption, the Gibbs energy was used, because the entropy change is very large in these process and because the entropy change mainly comes from the entropy in the gas phase, which can be evaluated in a usual manner.

For all these 3d metal particles, NO molecular adsorption is exergonic, as shown in Figure 2. The end-on adsorption energy increases in the order of $Cu_{55} \ll Ni_{55} < Fe_{55} \leq Co_{55}$. The side-on adsorption structure **2** is moderately less stable than the end-on adsorption **1**. The energy of transition state E(TS), defined as the difference in potential energy between the transition state and the sum of reactants (M_{55} + NO), becomes higher in the order of $Fe_{55} < Co_{55} < Ni_{55} \ll Cu_{55}$ (Figure 2 and Table 1), where the energy of **TS2** is shown for Co_{55} and Ni_{55} because **TS2** exists at a moderately lower energy than **TS1**. The activation barrier (E_a), defined as the difference in potential energy between the TS and the most stable NO

https://dx.doi.org/10.1021/acsomega.0c05838
ACS Omega 2021, 6, 4888−4898

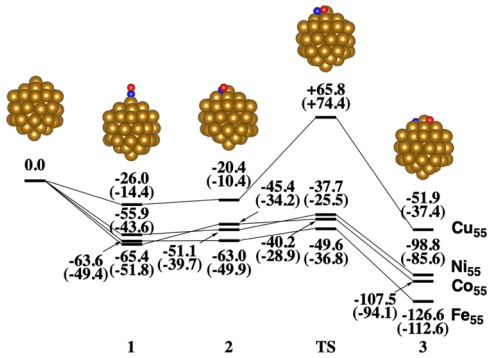

Figure 2. Energy changes[a] in NO dissociative adsorption onto M_{55} particles (M = Fe, Co, Ni, and Cu). Energies are shown in kcal mol^{-1} unit. For Co and Ni cases, the energy of **TS2** is shown because **TS2** is more stable in energy than **TS1**. [a]Potential energies without correction of zero-point energy are presented without parentheses; the Gibbs energies are presented in parentheses. The Gibbs energy changes are approximately evaluated, as described in the section "Computational Details and Models".

Table 1. Activation Barrier (E_a), Energy of Transition State (E(TS)), and Reaction Energy (ΔE) of NO Dissociative Adsorption onto 3d and 4d Metal Particles

	group			
	VIII	IX	X	XI
	Fe	Co	Ni	Cu
E_a[a]	14.0	25.2[d] (27.6)[e]	18.2[d] (22.2)[e]	90.4
E(TS)[b]	−49.6	−40.2[d] (−37.8)[e]	−37.7[d] (−33.7)[e]	+65.8
ΔE[c]	−126.6	−107.5	−98.8	−51.9
	group			
	VIII	IX	X	XI
	Ru[f]	Rh[f]	Pd[f]	Ag[f]
E_a[a]	27.0	38.7	80.8	115.5
E(TS)[b]	−45.0	−23.5	+34.3	+103.0
ΔE[c]	−124.0	−99.7	−60.0	+16.5

[a]Activation barrier (kcal mol^{-1}) defined as the energy difference between the transition state and the most stable intermediate before the transition state, where the potential energy without correction of zero-point energy is used. [b]Energy of transition state relative to the sum of M_{55} and NO. [c]Reaction energy defined as the energy difference between the product and the sum of M_{55} and NO. [d]For lower energy **TS2**. [e]For higher energy **TS1**. [f]Cited from ref 39.

molecular adsorption species **1**, increases in the order of Fe_{55} < Ni_{55} < Co_{55} ≪ Cu_{55}, almost identical to that of E(TS), except for the different orders of Co_{55} and Ni_{55}, as presented in Table 1. The difference between the order of E_a and that of E(TS) for Co_{55} and Ni_{55} is attributable to the larger NO end-on adsorption energy to Co_{55} than that to Ni_{55}. It is noteworthy that **TS3** of the reaction on Cu_{55} is calculated at a much higher Gibbs energy than the sum of reactants (Cu_{55} + NO). By contrast, for the other metal particles, TS is calculated at a lower Gibbs energy than the reactant (Figure 2). Consequently, it should be concluded that NO dissociative adsorption occurs on Fe, Co, and Ni particles but not on Cu particles even though **3** is more stable than the reactant in the Cu case. This conclusion agrees with experimental results.[12] In addition, it is noteworthy too that the Ni metal is reactive but Pd metal is not,[39] as reported from experiments,[12] although both belong to group X. This contrast between Ni and Pd metals is discussed below.

The reaction is markedly exothermic compared to both the sum of reactants (M_{55} + NO) and the most stable NO adsorption structure **1**. The reaction energy ΔE increases (becomes more negative) in the order of Cu_{55} ≪ Ni_{55} < Co_{55} < Fe_{55}. This order is the same as the decreasing order of E(TS), as expected from the Hammond rule, leading one to infer that the reactivity for NO dissociative adsorption increases in the same order both kinetically and thermodynamically; the same conclusion is obtained based on the Gibbs energy changes, as described in page S8 of the Supporting Information.

The other important result is that the E(TS) value is higher and the E_a value is larger in the 4d metal case than in the 3d metal case, when a comparison is made in the same group of the periodic table (Table 1). The ΔE values of Fe_{55} and Co_{55} are moderate to somewhat more negative than those of Ru_{55} and Rh_{55}. The ΔE values of Ni_{55} and Cu_{55} are considerably more negative than those of Pd_{55} and Ag_{55}. Consequently, one can conclude that the 3d metal particle is more reactive than the 4d metal particle in the same group of the periodic table both kinetically and thermodynamically.

Changes in Electron Distribution in NO Dissociative Adsorption. For better understanding NO dissociative adsorption, we investigated the changes in atomic charge by NO dissociative adsorption using Bader charges. In the end-on adsorption structure, the NO molecule is strongly negatively charged, as shown in Table 2. The negative charge is

Table 2. Changes in the Bader Charge (in e) by NO Dissociative Adsorption onto M_{55} (M = Fe, Co, Ni, and Cu)

			TS		
	1	2	TS1	TS2	3
			Fe_{55}−NO		
q(NO)	−0.365	−0.978	−1.170		−1.978
q(N)	+0.099	−0.422	−0.491		−0.929
q(O)	−0.464	−0.536	−0.679		−1.049
			Co_{55}−NO		
q(NO)	−0.338	−0.731	−1.160	−1.241	−1.815
q(N)	+0.268	−0.144	−0.491	−0.594	−0.887
q(O)	−0.606	−0.587	−0.669	−0.647	−0.927
			Ni_{55}−NO		
q(NO)	−0.233	−0.462	−1.123	−1.132	−1.682
q(N)	+0.143	+0.014	−0.464	−0.476	−0.809
q(O)	−0.376	−0.476	−0.659	−0.656	−0.872
			Cu_{55}−NO		
q(NO)	−0.256	−0.466		−1.036[a]	−1.874
q(N)	+0.126	+0.059		−0.362[a]	−0.922
q(O)	−0.382	−0.525		−0.676[a]	−0.951

[a]Bader charge at **TS3**.

considerably larger in the side-on adsorption structure **2** than in the end-on one **1**, indicating that charge transfer (CT) occurs from the metal particle to the NO molecule and that it is much larger in the side-on than in the end-on. The larger CT in the side-on than in the end-on is reasonable because one completely empty π^* orbital of NO overlaps more with the d-valence band in the side-on adsorption structure than in the end-on. This explanation is understood by considering that the π^* orbital in the M−N−O plane overlaps well with the M d orbitals in the case of the side-on structure but does not well in

https://dx.doi.org/10.1021/acsomega.0c05838
ACS Omega 2021, 6, 4888−4898

the end-on structure. The negative charge of NO increases further when going from **2** to **3** through **TS**. This finding is consistent with our understanding that the CT to anti-bonding MO plays an important role in σ-bond cleavage.[45] At **TS1**, the NO negative charge increases in the order of Cu_{55} < Ni_{55} < Co_{55} < Fe_{55}, in reverse to the increasing order of TS energy E(TS) (Table 1). Although **TS2** is moderately more stable than **TS1** for the Co and Ni cases, we employed **TS1** here for comparing the NO charge among Fe, Co, and Ni cases because CT depends considerably on the TS structure, as indicated by the NO charge of the Co and Ni cases at **TS1** and **TS2**. This comparison is not unreasonable because E(TS) does not differ much between **TS1** and **TS2**. Actually, the increasing order of E(TS) does not change even if we use **TS2** for comparing the Co and Ni cases with the Fe case. In the 4d metal case, the NO negative charge at TS is also related to the reactivity of M_{55} (M = Ru, Rh, and Pd) for N−O bond cleavage, except for Ag_{55}. These results of NO negative charges at **2**, **TS**, and **3** suggest that the CT from M_{55} to NO is a determining factor of reactivity for the N−O bond cleavage. In the lower energy **TS2** of Co and Ni cases, the NO molecule is more negatively charged than in **TS1**. The **TS2** geometry is likely to be more favorable for CT interaction with M_{55} than the **TS1** would be. In the reaction on Fe_{55}, only **TS1** was located, but **TS2** could not be, suggesting that the reaction on Fe_{55} need not have the **TS2** geometry because Fe_{55} can have strong CT interactions with NO even in **TS1**. However, the reactions on Co_{55} and Ni_{55} need to have the **TS2** geometry to have strong CT interactions because Co_{55} and Ni_{55} are less favorable for the CT than Fe_{55} is, as discussed below.

In product **3**, N and O atoms, respectively, have negative charges of −0.81 to −0.93 and −0.87 to −1.0 e. Their negative charges increase in the order of Ni_{55} < Co_{55} < Cu_{55} < Fe_{55}. This order is parallel to the increasing order (becoming more negative) of ΔE, except for Cu_{55}, suggesting that the large negative charges of the N and O atoms in **3** are related to the larger (more negative) ΔE value, the reason of which is discussed in the next section. However, the Cu case is exceptional because the N and O atoms are more negatively charged at **3** in the Cu case than in the Co and Ni cases (Table 3) despite its much smaller ΔE than in the Co and Ni cases (Table 1). This is a seemingly unreasonable discrepancy of the Cu case, but it is attributable to the electronic structure, as we discuss below.

Table 3. d-Valence Band-Top Energy ε(d-top),[a] d-Band Center Energy ε(d-c),[a] M_{55}−N and M_{55}−O Bond Energies BDE(M_{55}−N), and BDE(M_{55}−O)[b] (M = Fe, Co, Ni, Cu, Ru, Rh, Pd, and Ag)[c]

	Fe	Co	Ni	Cu
ε(d-top)	−3.30	−3.20	−3.60	−5.40 (s: −3.60)[d]
ε(d-c)	−5.00	−5.67	−6.27	−7.21
BDE(M_{55}−N)	142.7	129.0	130.1	100.8
BDE(M_{55}−O)	150.1	137.6	133.7	117.4
	Ru	Rh	Pd	Ag
ε(d-top)	−3.40	−3.70	−4.00	−6.80 (s: −3.30)[d]
ε(d-c)	−6.70	−6.59	−6.27	−8.43
BDE(M_{55}−N)	146.9	134.7	118.8	62.6
BDE(M_{55}−O)	174.7	123.5	105.9	87.4

[a]In eV. ε(d-c) is calculated using d-valence band. [b]BDE(M_{55}−X) (X = N or O) = E_t(M_{55}) + E_t(X) − E_t(M_{55}−X), where X = N or O and E_t is the total energy (in kcal mol^{-1}). [c]From ref 39 for 4d metals. [d]s-Band top energy.

Electronic Structure of M_{55} (M = Fe, Co, Ni, and Cu). The CT from M_{55} to NO generally depends on the energy level of the valence band. Therefore, we investigated the density of states (DOS) and the partial DOSs (PDOS). As shown in Figure 3, Fe_{55} and Co_{55} exhibit very large spin polarization because their 3d-shells are not fully occupied. By contrast, the spin polarization is moderate in Ni_{55} and tiny in Cu_{55} because their 3d-shells are, respectively, almost and completely occupied. The d-band center, which is calculated using d-valence band, is found at the very low energy in Cu_{55} and its energy ε(d-c) becomes higher in the order of Cu_{55} ≪ Ni_{55} < Co_{55} < Fe_{55}, as shown in Figure 3 and as presented in Table 3. The d-valence band-top energy ε(d-top) is also very low in Cu_{55}, where the first peak of DOS is defined as the band-top. It then rises following the same order. In the Cu case, the valence band-top exists at high energies, similarly to that of Ni_{55}, but it is not a 3d band but a 4s band. The presence of the 4s-valence band-top in the Cu case differs completely from the 3d-valence band-top of other particles, which arises from a $3d^{10}4s^1$ electron configuration of the Cu atom at the ground state. In other words, the difference in electron configuration is the reason why the results of Cu case differ considerably from those of other metal particles. Details are discussed below.

The CT quantity at **TS1** is parallel to the orders of ε(d-top) and ε(d-c) (Tables 2 and 3). In addition, the sum of negative charges of N and O atoms of **3** increases (more negative) in the order of Ni_{55} < Co_{55} < Fe_{55}, which is parallel to the orders of ε(d-top) and ε(d-c). These results suggest that the 3d valence orbital energy is an important property for determining the reactivity of M_{55}. It is noteworthy that the Cu case is excluded from the discussion presented above because its electronic structure differs completely from those of the others.

The 3d metal particle has higher energy ε(d-top) than the 4d metal particle does when a comparison is made in the same group of the periodic table. However, the ε(d-c) of Pd_{55} is almost identical to that of Ni_{55} (Table 3), although the ε(d-c) values of the other 3d metal particles are higher than those of the other 4d metals of the same group. Based on these results, one can reasonably conclude that the ε(d-c) does not always explain the difference in reactivity between 3d and 4d metal particles; moreover, the ε(d-top) is better for discussion than the ε(d-c). We use the ε(d-top) for discussion hereinafter. Because of this higher energy ε(d-top), the 3d metal particle forms stronger CT to the NO moiety from the metal particle than the 4d metal. The CT to anti-bonding MO is needed in σ-bond cleavage.[45] Therefore, the smaller E_a and lower energy E(TS) of the 3d metal particle than those of the 4d metal particle (Table 1) are inferred to arise from the higher energy ε(d-top) of the 3d metal particle.

Another important feature is that the ε(d-top) decreases from Fe to Cu, from Ru to Ag, and from the 3d metal to the 4d metal (Table 3). These features are consistent with the general trends observed for 3d and 4d orbital energies of metal atoms[44−46] and the d-ionization potentials of 3d and 4d metal atoms.[47] Because of these general features observed in the periodic table, it can be said that the reactivity of metal particles for NO dissociative adsorption decreases from Fe to Cu, from Ru to Ag, and from a 3d to a 4d metal in the same group of the periodic table.

https://dx.doi.org/10.1021/acsomega.0c05838
ACS Omega 2021, 6, 4888−4898

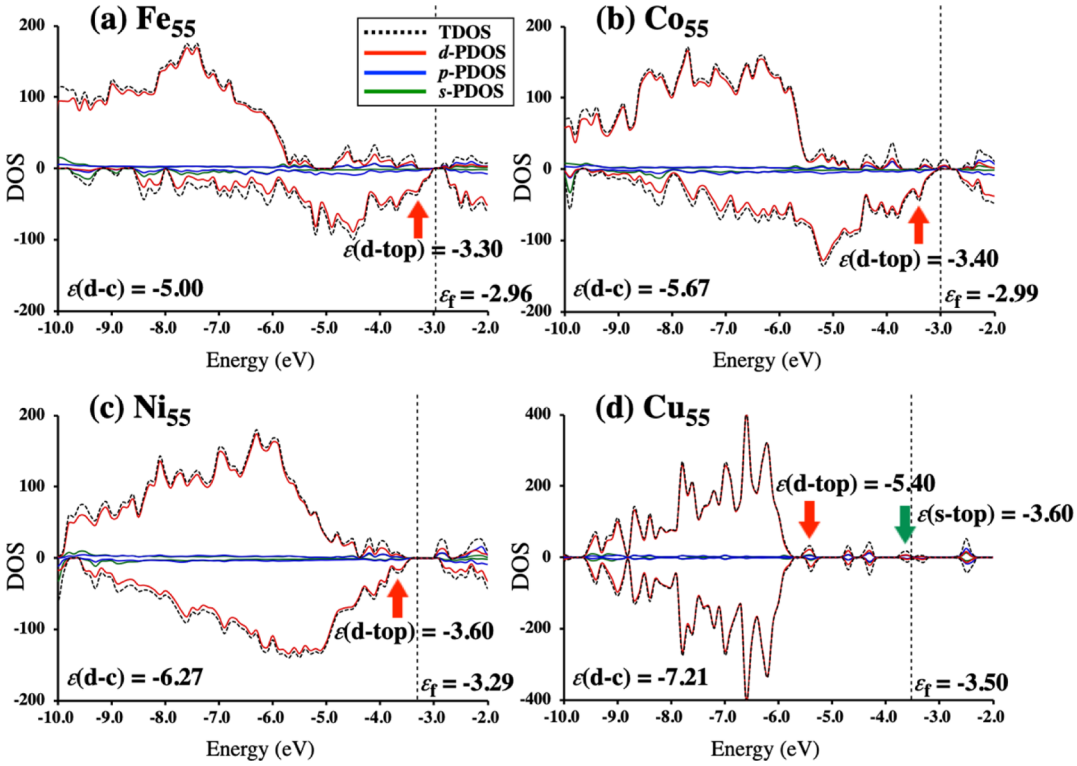

Figure 3. DOS and PDOS of s, p, and d bands of Fe_{55}, Co_{55}, Ni_{55}, and Cu_{55} particles. Energies of d-valence band top (red arrow), s-band top (green arrow), and d-band center (in eV) are represented, respectively, as ε(d-top), ε(s-top), and ε(d-c). The Fermi level is shown as a dashed line. ε(d-c) is calculated using d-valence band.

At the end of this section, we discuss several features of Cu_{55} that are different from those of Fe_{55}, Co_{55}, and Ni_{55}. The first of those different features is the smaller Cu−N−O angle of the NO adsorption structure than the M−N−O angle of the other M_{55} particles. Because the Cu atom has a $3d^{10}4s^1$ electron configuration in the ground state, the valence band-top consists of a Cu 4s orbital, as discussed above (Figure 3). The NO molecule has a lone-pair orbital on the N atom, one singly occupied π^* orbital, and the other empty π^* orbital. In the on-top end-on adsorption structure, the lone-pair orbital forms σ-donation to the conduction band and the π^* orbital forms back-donation from the d-valence band, as discussed earlier.[48,49] Fe_{55}, Co_{55}, and Ni_{55} have low-energy conduction bands consisting of 3d, 4s, and 4p orbitals around −2.5 eV in Fe_{55} and Co_{55} and −2.8 eV in Ni_{55}. However, Cu_{55} has it around −2.4 eV, a little bit higher energy than in the other metal particles. In addition, the DOS of the low-energy conduction band becomes smaller in the order of Fe_{55} > Co_{55} > Ni_{55} > Cu_{55}; it is particularly small in Cu_{55}. This feature arises from the increasing order of the number of valence electrons, Fe < Co < Ni < Cu. In other words, the very small low-energy conduction band of Cu_{55} is attributable to a fully occupied 3d-shell ($3d^{10}$ electron configuration) and the presence of one 4s electron. These features of Cu_{55} are not favorable for the CT from the lone-pair orbital of NO to Cu_{55}. Instead, the lone-pair orbital of NO gives rise to the exchange repulsion with the 4s-type valence band-top of Cu_{55} when the Cu−N−O angle is 180°. To reduce the exchange repulsion, NO changes the direction of the lone pair orbital by decreasing the Cu−N−O angle. In addition, the CT from NO to Cu_{55} is weak because the conduction band exists at a higher energy and its DOS is smaller than those of Ni_{55}. Accordingly, the negative charge of the NO moiety becomes larger than in the Ni_{55} case. In product **3** of the Cu case, the sum of N and O atomic charges is more negative than those of the Co and Ni cases despite the considerably smaller (less negative) ΔE than those of the Co and Ni cases. The more negatively charged N and O atoms of **3** in the Cu case are also attributed to the presence of the 4s-conduction band-bottom at the high energy and its small DOS because the CT from the N and O atoms to Cu_{55} is weak in such a case. These results show that the high-energy 4s-valence band-top and 4s-conduction band-bottom and the small DOS of the 4s-conduction band-bottom are origins of the different features of Cu case from other particles such as the smaller Cu−N−O angle, the more negatively charged NO in **1**, and more negatively charged N and O atoms in **3**.

Reaction Energy of NO Dissociative Adsorption and DOS Features. The reaction energy ΔE is related strongly to the M_{55}−N and M_{55}−O bond energies. Therefore, those bond energies are one of the important factors for NO dissociative adsorption. The sum of those bond energies decreases in the order of Fe_{55} > Co_{55} > Ni_{55} > Cu_{55}, as shown in Table 3, identically to the decreasing order of the ΔE value (Table 1). Here, the M_{55}−X (X = N or O) bond energy is defined as a difference between the total energy of M_{55}−X and the sum of total energies of M_{55} and X. In addition, the sum of those bond energies is smaller in the 4d metal particles than in the 3d metal particles except for the Fe and Ru cases (Table 3), which is consistent with the smaller (less negative) ΔE of the reaction with 4d metal particles than that of the reaction with 3d metal particles (Table 1).

The discussion of whether these bond energies depend on the d valence orbital energy is important. The bond energy of a

https://dx.doi.org/10.1021/acsomega.0c05838
ACS Omega 2021, 6, 4888−4898

polarized covalent bond is represented approximately by eq 1 based on the simple Hückel method,[50]

$$\mathrm{BDE}_{\mathrm{cov}} = \{(\varepsilon_{\mathrm{A}} - \varepsilon_{\mathrm{B}})^2 + 4\beta^2\}^{1/2} \quad (1)$$

where ε_A and ε_B, respectively, denote the Coulomb integrals of A and B atoms and β is the resonance integral. This equation is consistent with our understanding that the covalent bond becomes stronger when the difference in electronegativity increases between A and B atoms. The M−alkyl, M−silyl, and similar bonds (M = transition metal atom)[51−56] and the binding energy of oxygen-containing species with metal particles[39,57,58] are discussed and analyzed using this eq 1. It is likely that the β does not differ much among the M_{55} particles investigated here because all these atoms belong to the first-row late-transition-metal elements. In such a case, the larger $\varepsilon_A-\varepsilon_B$ term engenders the larger A−B bond energy and more negatively charged N and O atoms in **3**. Based on this understanding, eq 1 provides a reasonable explanation for the decreasing order of M−N and M−O bond energies Fe_{55} > Co_{55} > Ni_{55} and the same decreasing order of the negative charge, as follows. The Coulomb integral ε_A approximately corresponds to the valence orbital energy. The metal 3d valence orbital exists at a higher energy than the 2p valence orbitals of N and O atoms, as shown in Scheme 2, because of the much smaller electronegativity of the 3d metal element than those of N and O atoms. Because the highest energy d valence orbital mainly contributes to the M_{55}−X bond according to frontier orbital theory and because the ε(d-top) becomes lower when going from Fe to Ni, as discussed above, the $\varepsilon_A-\varepsilon_B$ term decreases when going from Fe to Ni, resulting in the same decreasing orders of M_{55}−N and M_{55}−O bond energies and the negative charges of N and O atoms in **3**, as shown in Table 3.

Scheme 2. Orbital Energy Diagram between the d-Valence Band-Top and 2p Orbital of N or O Atoms

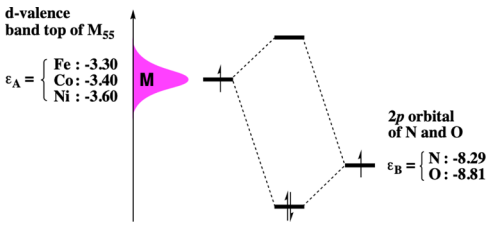

The Cu case was excluded from the discussion presented above. Next, we must discuss the reason why the Cu_{55}−N and Cu_{55}−O bond energies are much smaller than those of Ni_{55} despite the presence of Cu_{55} 4s valence band a high energy. For Ag_{55}, we encountered the same problem showing that the Ag_{55}−N and Ag_{55}−O bond energies are much smaller than those of Pd_{55}, Rh_{55}, and Ru_{55} despite the presence of a Ag_{55} 5s valence band a high energy.[39] Because of the d^{10} electron configuration, the d-shell of Cu and Ag does not contribute to the metal−metal bond. In such a case, the metal−metal bond is formed only by s electrons. The Cu atom has only one 4s valence electron, which is mainly used for the Cu−Cu bonding interaction. Therefore, the 4s electron cannot contribute greatly to the Cu_{55}−N and Cu_{55}−O bonds. For this reason, Cu_{55}−N and Cu_{55}−O bonds are weaker than the other M_{55}−N and M_{55}−O bonds. We shall end the discussion here because an almost identical explanation has been presented for the Ag case.[39]

Similarities and Differences between 3d and 4d Metal Particles for NO Dissociative Adsorption. As described in the "Introduction" section, Co is reactive for NO dissociative adsorption, similar to Rh in group IX. Moreover, Cu is not reactive like Ag in group XI. However, in group X, Ni is reactive but Pd is not. These experimentally obtained observations[12] are reproduced by the present density functional theory (DFT) calculations. One would reasonably wonder why the reactivity is similar between 3d and 4d metals in groups IX and XI but different in group X. Two important trends should be remembered; in one, the d orbital energy lowers when going from the left-hand side to the right-hand side in the periodic table; while in the other, the 3d orbital exists at a higher energy than the 4d orbital. Consequently, the reactivity of metal particles for NO dissociative adsorption decreases from Fe to Cu, from Ru to Ag, and also from the 3d metal element to the 4d element in the same group. Because of these trends, the reactivity disappears at group XI (Cu) in the 3d metal, but at an earlier group X (Pd) in the 4d metal.

This discussion suggests that the reactivity of the Ni particle differs greatly from that of the Pd particle but rather resembles that of the Rh particle. The reactivity of the Co particle rather resembles that of the Ru particle because of the similarity of ε(d-top). In other words, the left-low diagonal similarity exists between group X of the 3d metal (Ni) and group IX of the 4d metal (Rh) and between group IX of the 3d metal (Co) and group VIII of the 4d metal (Ru). This similarity is possible when ε(d-top) plays an important role in determining the reactivity. This left-low diagonal similarity differs from the right-low diagonal similarity in the periodic table between the first and the second series p-block elements because the right-low diagonal similarity of p-block elements arises from a similar atomic radius, charge density, and electronegativity.

■ CONCLUSIONS

The NO dissociative adsorption onto 3d metal particles M_{55} (M = Fe, Co, Ni, and Cu) was investigated theoretically. DFT computations here clearly show that NO dissociative adsorption occurs on M = Fe, Co, and Ni (group VIII to X) but not on M = Cu (group X). These results agree with the experimentally obtained findings.[12] It is noteworthy that Ni_{55} is reactive for NO dissociative adsorption but Pd_{55} is not, although both belong to the same group X. The transition state becomes lower in energy in the order of $Cu_{55} \gg Ni_{55} > Co_{55} > Fe_{55}$ and the reaction energy increases (becomes more negative) in the order of $Cu_{55} \ll Ni_{55} < Co_{55} < Fe_{55}$, indicating that the reactivity for NO dissociative adsorption increases in the same order both kinetically and thermodynamically.

When going from the reactant (M_{55} + NO) to the product (adsorbed N and O atoms), the negative charge of the NO moiety increases. The negative charge of the NO moiety at the transition state increases in the order of $Ni_{55} < Co_{55} < Fe_{55}$, when a comparison is made in the same kind of transition-state structure (**TS1**). These results indicate that the CT from the metal particle to NO plays an important role in NO dissociative adsorption. This increasing order is parallel to the increasing order of the d-valence band-top energy ε(d-top).

The other important factor is the reaction energy, which is determined by the M_{55}−N and M_{55}−O bond energies. The sum of bond energies increases in the order of $Cu_{55} < Ni_{55} <$

https://dx.doi.org/10.1021/acsomega.0c05838
ACS Omega 2021, 6, 4888−4898

Co_{55} < Fe_{55}. These bond energies increase as the d valence band-top rises in energy. Because the ε(d-top) lowers in the order of Fe > Co > Ni, which is the same as the fundamental characteristics of the periodic table,[46,47] the M_{55}−N and M_{55}−O bonds strengthen in the order of Ni < Co < Fe. The weak Cu_{55}−N and Cu_{55}−O bonds arise from the $3d^{10}4s^1$ electron configuration of the Cu atom.

Summarizing the results of CT from M_{55} to NO and the M_{55}−N and M_{55}−O bond energies, it should be concluded that ε(d-top) is an important property to determining the reactivity for NO dissociative adsorption in both kinetics and thermodynamics. This ε(d-top) becomes lower when going from Fe to Cu, from Ru to Ag, and from the 3d metal to the 4d metal in the same group. These features are the origin of the reactivity trend of these 3d and 4d metal particles.

At the end of this section, the Cu case must be mentioned because its differs greatly from the other particles; (i) it is not reactive for NO dissociative adsorption; (ii) the Cu_{55}−N and Cu_{55}−O bonds are weaker than those of the other metals; and (iii) its 4s valence band-top exists at a similar energy to the 3d valence band-top of Ni_{55}, but the d valence band-top exists at much lower energy than the other metal particles. These features are mutually consistent. However, **3** has more negatively charged N and O atoms in the Cu case than in either the Co or Ni case. These more negatively charged N and O atoms in **3** are seemingly inconsistent with the smaller (less negative) reaction energy and smaller Cu_{55}−N and Cu_{55}−O bond energies. The reason for that apparent inconsistency is the presence of the 4s conduction band-bottom at high energies and its small DOS. These features are not favorable for the CT from N and O atoms to Cu_{55}. Therefore, much negative charge remains on the N and O atoms. The weak Cu_{55}−N and Cu_{55}−O bonds arise from the $3d^{10}4s^1$ electron configuration of the Cu atom. Because of the $3d^{10}4s^1$ electron configuration, the 3d band does not contribute to the Cu−Cu bond. Only the singly occupied 4s valence shell contributes to the Cu−Cu bond. Consequently, the Cu 4s shell does not contribute well to the Cu_{55}−NO, Cu_{55}−N, and Cu_{55}−O bonds, which result in lower reactivity, smaller Cu_{55}−N and Cu_{55}−O bond energies, and smaller exothermicity of NO dissociative adsorption, but more negatively charged N and O atoms in **3** than those of the other Co_{55} and Ni_{55} particles.

■ COMPUTATIONAL DETAILS AND MODELS

Spin-polarized DFT was used with the Perdew−Burke−Ernzerhof (PBE) functional[59] using plane-wave basis sets for representing valence electrons with an energy cutoff of 400 eV and the projector-augmented wave method for representing core electrons.[60,61] The dispersion correction influences slight energy changes in NO dissociative adsorption onto 3d metal particles M_{55}, as shown in Table S4 of the Supporting Information. The HSE06 functional was employed for calculating the DOS[62] because this functional provides a better band-gap in general. The Monkhorst−Pack grid method was used for 1 × 1 × 1 *k*-point sampling. The metal particle was placed at the center of a 25 × 25 × 25 Å cubic box under the periodic boundary condition, which seems sufficient to neglect the interaction between the metal particle and its periodic image. In geometry optimization, convergence criteria for total energy and maximum force were set, respectively, to 1.0×10^{-4} eV and 0.01 eV/Å. The transition state was optimized using the nudged elastic band method.[63,64] Vibrational frequencies were calculated for all optimized geometries to check that the transition state has one imaginary frequency and that equilibrium geometry has no imaginary frequency, where the NO moiety, N and O atoms, one vertex M atom interacting with the NO moiety, and five M atoms surrounding the vertex M atom are involved in the calculation while the other part was fixed. This approximation was employed here to reduce the computational time because frequency calculations are very time-consuming. In this approximation, many M−M vibrations are neglected, indicating that the Gibbs energy and zero-point energy evaluated by this procedure are approximated values. However, it is likely that this procedure provides important frequencies for understanding whether a species has an equilibrium structure or a transition state. Because of this approximation, we mainly used the potential energy without zero-point energy correction for discussion and used the Gibbs energy only for discussing which of NO desorption and NO dissociative adsorption occurs; remember that the entropy change is very large in adsorption and desorption. All these DFT calculations were conducted using the Vienna ab initio simulation package.[65,66]

We used M_{55} as a model of metal particles because this particle has been used in the recent theoretical study of NO dissociative adsorption to several 4d metal particles.[39] Although M_{55} metal particles are small compared to most real catalysts, the use of M_{55} particle is not so unreasonable because they are of sub-nanometer scale and because M_{55} metal particles have been employed as model catalysts in theoretical studies of heterogeneous catalytic reactions and related reactions.[37,57,67−74] Also, a recent theoretical study of NO dissociative adsorption onto Rh_{55}, Rh_{147}, and Rh(111) surfaces has indicated that the activation barrier differs little among them and that the reaction energy of the Rh_{55} case is moderately larger (more exothermic) than those of the others, but it does not differ very much.[37] It is likely that the comparison is reasonably made using M_{55} among Fe, Co, Ni, and Cu particles and between the 3d metal and 4d metal particles in the same group, although M_{55} is smaller than real metal particles.

As shown in Schemes 1a and S1 of the Supporting Information, this particle has symmetrical structures of two kinds: icosahedral (I_h) and octahedral (O_h) structures. In our recent work, we used the I_h structure of a 4d metal particle M_{55} in theoretical calculations of NO dissociative adsorption because the I_h structure is more stable than the O_h in Ru_{55}, Rh_{55}, Pd_{55}, and Ag_{55}.[39] We also investigated the relative stabilities of I_h and O_h structures of the 3d metal particle M_{55}, which revealed that the I_h structure is more stable than the O_h in Fe_{55}, Co_{55}, Ni_{55}, and Cu_{55} too. Table S5 of the Supporting Information presents their relative energies. Therefore, we used the I_h structure of M_{55} and made comparisons of reactivity and electronic structure between 3d and 4d metals. It is noteworthy that the comparison must be made using the same surface structure because the reactivity toward the NO molecule depends on the metal surface structure.[12]

In the I_h structure of M_{55}, 42 M atoms exist on the surface. The surface has 30 M atoms at the edge position and 12 M atoms at the vertex position (Scheme 1b). NO adsorption and NO reaction were investigated at these possible adsorption positions. Geometries of intermediate and transition states were optimized with no constraint, starting from the I_h-like geometry.

https://dx.doi.org/10.1021/acsomega.0c05838
ACS Omega 2021, 6, 4888−4898

■ ASSOCIATED CONTENT

Supporting Information

The Supporting Information is available free of charge at https://pubs.acs.org/doi/10.1021/acsomega.0c05838.

Octahedral structure of M_{55}; NO adsorption onto vertex and edge positions; spin-polarization M_{55}; comparison of the NO frequency between the computational value and the experimental one; comparison of energy changes in NO dissociative adsorption between PBE and PBE-D3 functionals; relative stabilities of I_h and O_h structures of M_{55}; and Cartesian coordinates of the optimized structures (PDF)

■ AUTHOR INFORMATION

Corresponding Author

Shigeyoshi Sakaki − *Elements Strategy Initiative for Catalysts and Batteries, Kyoto University, Kyoto 615-8245, Japan;* orcid.org/0000-0002-1783-3282; Email: sakaki.shigeyoshi.47e@st.kyoto-u.ac.jp

Authors

Nozomi Takagi − *Elements Strategy Initiative for Catalysts and Batteries, Kyoto University, Kyoto 615-8245, Japan*

Masahiro Ehara − *Elements Strategy Initiative for Catalysts and Batteries, Kyoto University, Kyoto 615-8245, Japan; Institute for Molecular Science, Okazaki 444-8585, Japan;* orcid.org/0000-0002-2185-0077

Complete contact information is available at: https://pubs.acs.org/10.1021/acsomega.0c05838

Author Contributions

N.T. performed the calculations, summarized the computational results, and drafted the manuscript. S.S., M.E., and N.T. analyzed the computational results and found important features. S.S. conceived the research study, coordinated, and finalized the manuscript. All the authors read and approved the final manuscript.

Notes

The authors declare no competing financial interest.

■ ACKNOWLEDGMENTS

This work was mainly carried out under the project "Element Strategy Initiative for Catalysts and Batteries (ESICB)", which is financially supported by the Ministry of Education, Culture, Science, Sports, and Technology (MEXT), Japan. S.S. is thankful to JST CREST, grant number JPMJCR20B6, Japan, for partial financial support. N.T. is thankful to JSPS KAKENHI grant number 19K05386 for partial financial support. We wish to thank the computational center at the Institute of Molecular Science (Okazaki, Japan) and the High-Performance Computing Infrastructure (HPCI; Kobe, Japan) for allowing us to use supercomputers (no. hp200039).

■ REFERENCES

(1) Taylor, K. C. Nitric Oxide Catalysis in Automotive Exhaust Systems. *Catal. Rev.* **1993**, *35*, 457−481.

(2) Kašpar, J.; Fornasiero, P.; Hickey, N. Automotive catalytic converters: current status and some perspectives. *Catal. Today* **2003**, *77*, 419−449.

(3) Bowker, M. Automotive catalysis studied by surface science. *Chem. Soc. Rev.* **2008**, *37*, 2204−2211.

(4) Granger, P.; Parvulescu, V. I. Catalytic NOx Abatement Systems for Mobile Sources: From Three-Way to Lean Burn after-Treatment Technologies. *Chem. Rev.* **2011**, *111*, 3155−3207.

(5) Wang, J.; Chen, H.; Hu, Z.; Yao, M.; Li, Y. A Review on the Pd-Based Three-Way Catalyst. *Catal. Rev.: Sci. Eng.* **2015**, *57*, 79−144.

(6) Beale, A. M.; Gao, F.; Lezcano-Gonzalez, I.; Peden, C. H. F.; Szanyi, J. Recent advances in automotive catalysis for NOx emission control by small-pore microporous materials. *Chem. Soc. Rev.* **2015**, *44*, 7371−7405.

(7) Kobylinski, T. P.; Taylor, B. W. The Catalytic Chemistry of Nitric Oxide: II. Reduction of Nitric Oxide over Noble Metal Catalysts. *J. Catal.* **1974**, *33*, 376−384.

(8) Shelef, M.; Graham, G. W. Why Rhodium in Automotive 3-Way Catalysts? *Catal. Rev.* **1994**, *36*, 433−457.

(9) Granger, P.; Dhainaut, F.; Pietrzik, S.; Malfoy, P.; Mamede, A. S.; Leclercq, L.; Leclercq, G. An Overview: Comparative Kinetic Behavior of Pt, Rh and Pd in the NO + CO and NO + H_2 Reactions. *Top. Catal.* **2006**, *39*, 65−76.

(10) Srinivasan, A.; Depcik, C. Review of Chemical Reactions in the NO Reduction by Co on Rhodium/Alumina Catalysts. *Catal. Rev.* **2010**, *52*, 462−493.

(11) Root, T. W.; Schmidt, L. D.; Fisher, G. B. Adsorption and Reaction of Nitric-Oxide and Oxygen on Rh(111). *Surf. Sci.* **1983**, *134*, 30−45.

(12) Brown, W. A.; King, D. A. NO Chemisorption and Reactions on Metal Surfaces: A New Perspective. *J. Phys. Chem. B* **2000**, *104*, 2578−2595.

(13) Garin, F. Mechanism of NO_x decomposition. *Appl. Catal., A* **2001**, *222*, 183−219.

(14) Anderson, M. L.; Ford, M. S.; Derrick, P. J.; Drewello, T.; Woodruff, D. P.; Mackenzie, S. R. Nitric Oxide Decomposition on Small Rhodium Clusters, $Rh_n^{+/-}$. *J. Phys. Chem. A* **2006**, *110*, 10992−11000.

(15) Tawaraya, Y.; Kudoh, S.; Miyajima, K.; Mafuné, F. Thermal Desorption and Reaction of NO Adsorbed on Rhodium Cluster Ions Studied by Thermal Desorption Spectroscopy. *J. Phys. Chem. A* **2015**, *119*, 8461−8468.

(16) Brown, W. A.; Sharma, R. K.; King, D. A.; Haq, S. Adsorption and Reactivity of NO and N_2O on Cu{110}: Combined RAIRS and Molecular Beam Studies. *J. Phys. Chem.* **1996**, *100*, 12559−12568.

(17) Dumas, P.; Suhren, M.; Chabal, Y. J.; Hirschmugl, C. J.; Williams, J. P. Adsorption and reactivity of NO on Cu(111): a synchrotron infrared reflection absorption spectroscopic study. *Surf. Sci.* **1997**, *371*, 200−212.

(18) Brown, W. A.; Gardner, P.; Jigato, M. P.; King, D. A. Characterization and orientation of adsorbed NO dimers on Ag{111} at low temperatures. *J. Chem. Phys.* **1995**, *102*, 7277−7280.

(19) Carley, A. F.; Davies, P. R.; Roberts, M. W.; Santra, A. K.; Thomas, K. K. Coadsorption of carbon monoxide and nitric oxide at Ag(111): evidence for a CO−NO surface complex. *Surf. Sci.* **1998**, *406*, L587−L591.

(20) Jigato, M. P.; Somasundram, K.; Termath, V.; Handy, N. C.; King, D. A. Vibrational frequencies for NO chemisorbed on different sites: DFT calculations on Pd clusters. *Surf. Sci.* **1997**, *380*, 83−90.

(21) Hammer, B.; Nørskov, J. K. Adsorbate Reorganization at Steps: NO on Pd(211). *Phys. Rev. Lett.* **1997**, *79*, 4441−4444.

(22) Loffreda, D.; Simon, D.; Sautet, P. Vibrational Frequency and Chemisorption Site: A DFT-Periodic Study of NO on Pd (111) and Rh (111) Surfaces. *Chem. Phys. Lett.* **1998**, *291*, 15−23.

(23) Loffreda, D.; Simon, D.; Sautet, P. Molecular and dissociative chemisorption of NO on palladium and rhodium (100) and (111) surfaces: A density-functional periodic study. *J. Chem. Phys.* **1998**, *108*, 6447.

(24) Ge, Q.; Brown, W. A.; Sharma, R. K.; King, D. A. NO monomer and (NO)x polymeric chain chemisorption on Pt{110}: Structure and energetics. *J. Chem. Phys.* **1999**, *110*, 12082.

(25) Hammer, B.; Hansen, L. B.; Nørskov, J. K. Improved adsorption energetics within density-functional theory using revised

Perdew-Burke-Ernzerhof functionals. *Phys. Rev. B: Condens. Matter Mater. Phys.* **1999**, *59*, 7413−7421.
(26) Jigato, M. P.; King, D. A.; Yoshimori, A. The chemisorption of spin polarised NO on Ag{111}. *Chem. Phys. Lett.* **1999**, *300*, 639−644.
(27) Mavrikakis, M.; Rempel, J.; Greeley, J.; Hansen, L. B.; Nørskov, J. K. Atomic and Molecular Adsorption on Rh(111). *J. Chem. Phys.* **2002**, *117*, 6737−6744.
(28) Bondino, F.; Comelli, G.; Baraldi, A.; Vesselli, E.; Rosei, R.; Goldoni, A.; Lizzit, S. NO adsorption on Rh(100). II. Stability of the adlayers. *J. Chem. Phys.* **2003**, *119*, 12534−12539.
(29) Popa, C.; Flipse, C. F. J.; Jansen, A. P. J.; van Santen, R. A.; Sautet, P. NO Structures Adsorbed on Rh(111): Theoretical Approach to High-Coverage STM Images. *Phys. Rev. B: Condens. Matter Mater. Phys.* **2006**, *73*, 245408.
(30) Tian, K.; Tu, X.-Y.; Dai, S.-S. NO dissociation pathways on Rh(100), (110), and (111) surfaces: A comparative density functional theory study. *Surf. Sci.* **2007**, *601*, 3186−3195.
(31) Popa, C.; van Bavel, A. P.; van Santen, R. A.; Flipse, C. F. J.; Jansen, A. P. J. Density Functional Theory Study of NO on the Rh(100) Surface. *Surf. Sci.* **2008**, *602*, 2189−2196.
(32) Wu, G.; Yang, M.; Guo, X.; Wang, J. Comparative DFT Study of N_2 and NO Adsorption on Vanadium Clusters V_n (n = 2−13). *J. Comput. Chem.* **2012**, *33*, 1854−1861.
(33) Hirai, T.; Okoshi, M.; Ishikawa, A.; Nakai, H. Temperature- and pressure-dependent adsorption configuration of NO molecules on Rh(111) surface: A theoretical study. *Surf. Sci.* **2019**, *686*, 58−62.
(34) Nanba, Y.; Koyama, M. NO Adsorption on 4d and 5d Transition-Metal (Rh, Pd, Ag, Ir, and Pt) Nanoparticles: Density Functional Theory Study and Supervised Learning. *J. Phys. Chem. C* **2019**, *123*, 28114−28122.
(35) de Amorim, R. V.; Batista, K. E. A.; Nagurniak, G. R.; Orenha, R. P.; Parreira, R. L. T.; Piotrowski, M. J. CO, NO, and SO adsorption on Ni nanoclusters: a DFT investigation. *Dalton Trans.* **2020**, *49*, 6407−6417.
(36) Matsumura, Y.; Koda, Y.; Yamada, H.; Shigetsu, M.; Takami, A.; Ishimoto, T.; Kai, H. Experimental and Computational Studies of CO and NO Adsorption Properties on Rh-Based Single Nanosized Catalysts. *J. Phys. Chem. C* **2020**, *124*, 2953−2960.
(37) Deushi, F.; Ishikawa, A.; Nakai, H. Density Functional Theory Analysis of Elementary Reactions in NOx Reduction on Rh Surfaces and Rh Clusters. *J. Phys. Chem. C* **2017**, *121*, 15272−15281.
(38) Ishikawa, A.; Tateyama, Y. First-Principles Microkinetic Analysis of NO + CO Reactions on Rh(111) Surface toward Understanding NOx Reduction Pathways. *J. Phys. Chem. C* **2018**, *122*, 17378−17388.
(39) Takagi, N.; Ishimura, K.; Fukuda, R.; Ehara, M.; Sakaki, S. Reaction Behavior of the NO Molecule on the Surface of an M_n Particle (M = Ru, Rh, Pd, and Ag; n = 13 and 55): Theoretical Study of Its Dependence on Transition-Metal Element. *J. Phys. Chem. A* **2019**, *123*, 7021−7033.
(40) Takagi, N.; Nakagaki, M.; Ishimura, K.; Fukuda, R.; Ehara, M.; Sakaki, S. Electronic Processes in NO Dimerization on Ag and Cu Clusters: DFT and MRMP2 Studies. *J. Comput. Chem.* **2019**, *40*, 181−190.
(41) Iwasa, T.; Sato, T.; Takagi, M.; Gao, M.; Lyalin, A.; Kobayashi, M.; Shimizu, K.-i.; Maeda, S.; Taketsugu, T. Combined Automated Reaction Pathway Searches and Sparse Modeling Analysis for Catalytic Properties of Lowest Energy Twins of Cu_{13}. *J. Phys. Chem. A* **2019**, *123*, 210−217.
(42) Takagi, N.; Ishimura, K.; Miura, H.; Shishido, T.; Fukuda, R.; Ehara, M.; Sakaki, S. Catalysis of Cu Cluster for NO Reduction by CO: Theoretical Insight into Reaction Mechanism. *ACS Omega* **2019**, *4*, 2596−2609.
(43) The radius of maximum charge density is 0.38, 0.35, and 0.33 a.u. for 3d orbitals of Fe, Co, and Ni, respectively. The radius is 1.2 a.u. for Cu 4s orbital. These are computational values with the relativistic Hartree−Fock method.[44]
(44) Fraga, S.; Saxena, K. M. S.; Karwowski, J. *Handbook of Atomic Data*; Elsevier: Amsterdam, 1976.
(45) Guan, W.; Sayyed, F. B.; Zeng, G.; Sakaki, S. σ-Bond Activation of Small Molecules and Reactions Catalyzed by Transition-Metal Complexes: Theoretical Understanding of Electronic Processes. *Inorg. Chem.* **2014**, *53*, 6444−6457.
(46) Sakaki, S. Theoretical and Computational Study of a Complex System Consisting of Transition Metal Element(s): How to Understand and Predict Its Geometry, Bonding Nature, Molecular Property, and Reaction Behavior. *Bull. Chem. Soc. Jpn.* **2015**, *88*, 889−938. and Supporting Information. The trend of d orbital energy is presented in the Supporting Information
(47) Emsley, J. *The Elements*, 3rd ed.; Oxford University Press, 1998. The 2'nd ionization potential of M^+ atom increases as going from the left-hand side to the right-hand side in the periodic table; the 1'st ionization potential occurs from the valence s electron of M^0 atom and the 2'nd ionization potential occurs from the valence d electron of M^+ atom.
(48) Vuckovic, D. L.; Jansen, S. A.; Hoffmann, R. Adsorption and Coadsorption of CO and NO on the Rh(100) Surface: A Theoretical Analysis. *Langmuir* **1990**, *6*, 732−746.
(49) Sung, S. S.; Hoffmann, R.; Thiel, P. A. NO Chemisorption on Ni(111): Coverage Effects, Site Preferences, and Adsorption Geometry. *J. Phys. Chem.* **1986**, *90*, 1380−1388.
(50) Sakaki, S.; Biswas, B.; Sugimoto, M. A Theoretical Study of the C−H Activation of Methane Derivatives. Significant Effects of Electron-Withdrawing Substituents. *Organometallics* **1998**, *17*, 1278−1289.
(51) Sakaki, S.; Kai, S.; Sugimoto, M. Theoretical Study on σ-Bond Activation of $(HO)_2B-XH_3$ by $M(PH_3)_2$ (X = C, Si, Ge, or Sn; M = Pd or Pt). Noteworthy Contribution of the Boryl p_π Orbital to M−Boryl Bonding and Activation of the B−X σ-Bond. *Organometallics* **1999**, *18*, 4825−4837.
(52) Biswas, B.; Sugimoto, M.; Sakaki, S. Theoretical Study of the Structure, Bonding Nature, and Reductive Elimination Reaction of $Pd(XH_3)(\eta^3\text{-}C_3H_5)(PH_3)$ (X=C, Si, Ge, Sn). Hypervalent Behavior of Group 14 Elements. *Organometallics* **1999**, *18*, 4015−4026.
(53) Ray, M.; Nakao, Y.; Sato, H.; Sakaba, H.; Sakaki, S. How to Stabilize η^3-Silapropargyl/Alkynylsilyl Complex of $[CpL_2M]^+$ (L = CO, PMe_3, or PF_3 and M = W or Mo): Theoretical Prediction. *Organometallics* **2009**, *28*, 65−73.
(54) Sugiyama, A.; Ohnishi, Y.-y.; Nakaoka, M.; Nakao, Y.; Sato, H.; Sakaki, S.; Nakao, Y.; Hiyama, T. Why Does Fluoride Anion Accelerate Transmetalation between Vinylsilane and Palladium(II)-Vinyl Complex? Theoretical Study. *J. Am. Chem. Soc.* **2008**, *130*, 12975−12985.
(55) Ray, M.; Nakao, Y.; Sato, H.; Sakaki, S. Theoretical Study of Tungsten η^3-Silaallyl/η^3-Vinylsilyl and Vinyl Silylene Complexes: Interesting Bonding Nature and Relative Stability. *Organometallics* **2007**, *26*, 4413−4423.
(56) Zhong, R.-L.; Sakaki, S. sp^3 C−H Borylation Catalyzed by Iridium(III) Triboryl Complex: Comprehensive Theoretical Study of Reactivity, Regioselectivity, and Prediction of Excellent Ligand. *J. Am. Chem. Soc.* **2019**, *141*, 9854−9866.
(57) Zhu, B.; Ehara, M.; Sakaki, S. Propene oxidation catalysis and electronic structure of M_{55} particles (M = Pd or Rh): differences and similarities between Pd_{55} and Rh_{55}. *Phys. Chem. Chem. Phys.* **2020**, *22*, 11783−11796.
(58) Lu, J.; Zhu, B.; Sakaki, S. O_2 activation by core−shell Ru_{13}@Pt_{42} particles in comparison with Pt_{55} particles: a DFT study. *RSC Adv.* **2020**, *10*, 36090−36100.
(59) Perdew, J. P.; Burke, K.; Ernzerhof, M. Generalized Gradient Approximation Made Simple. *Phys. Rev. Lett.* **1996**, *77*, 3865−3868.
(60) Blöchl, P. E. Projector augmented-wave method. *Phys. Rev. B: Condens. Matter Mater. Phys.* **1994**, *50*, 17953−17979.
(61) Kresse, G.; Joubert, D. From ultrasoft pseudopotentials to the projector augmented-wave method. *Phys. Rev. B: Condens. Matter Mater. Phys.* **1999**, *59*, 1758−1775.

https://dx.doi.org/10.1021/acsomega.0c05838
ACS Omega 2021, 6, 4888−4898

(62) Heyd, J.; Scuseria, G. E.; Ernzerhof, M. Hybrid functionals based on a screened Coulomb potential. *J. Chem. Phys.* **2003**, *118*, 8207.
(63) Mills, G.; Jónsson, H. Quantum and Thermal Effects in H_2 Dissociative Adsorption: Evaluation of Free Energy Barriers in Multidimensional Quantum Systems. *Phys. Rev. Lett.* **1994**, *72*, 1124−1127.
(64) Mills, G.; Jónsson, H.; Schenter, G. K. Reversible Work Transition State Theory: Application to Dissociative Adsorption of Hydrogen. *Surf. Sci.* **1995**, *324*, 305−337.
(65) Kresse, G.; Furthmüller, J. Efficiency of ab-initio total energy calculations for metals and semiconductors using a plane-wave basis set. *Comput. Mater. Sci.* **1996**, *6*, 15−50.
(66) Kresse, G.; Furthmüller, J. Efficient iterative schemes for *ab initio* total-energy calculations using a plane-wave basis set. *Phys. Rev. B: Condens. Matter Mater. Phys.* **1996**, *54*, 11169−11186.
(67) Cheng, D.; Wang, W. Tailoring of Pd−Pt bimetallic clusters with high stability for oxygen reduction reaction. *Nanoscale* **2012**, *4*, 2408−2415.
(68) Shin, J.; Choi, J.-H.; Bae, Y.-S.; Lee, S.-C. Effect of surface hydroxyl coverage on platinum nanoparticles in the oxygen reduction reaction: All-electron density functional theory analysis. *Chem. Phys. Lett.* **2014**, *610−611*, 86−90.
(69) Jennings, P. C.; Aleksandrov, H. A.; Neyman, K. M.; Johnston, R. L. A DFT study of oxygen dissociation on platinum based nanoparticles. *Nanoscale* **2014**, *6*, 1153−1165.
(70) Cheng, D.; Xu, H.; Fortunelli, A. Tuning the catalytic activity of Au−Pd nanoalloys in CO oxidation via composition. *J. Catal.* **2014**, *314*, 47−55.
(71) Ma, L.; Akola, J. Varying oxygen coverage on Cu_{55} and its effect on CO oxidation. *Phys. Chem. Chem. Phys.* **2019**, *21*, 11351−11358.
(72) Morishita, T.; Ueno, T.; Panomsuwan, G.; Hieda, J.; Antoaneta Bratescu, M.; Saito, N. DFT calculation of oxygen adsorption on a core-single shell ZnNb catalyst. *RSC Adv.* **2016**, *6*, 98091−98095.
(73) Batista, K. E. A.; Da Silva, J. L. F.; Piotrowski, M. J. Adsorption of CO, NO, and H_2 on the Pd_nAu_{55-n} Nanoclusters: A Density Functional Theory Investigation within the van der Waals D3 Corrections. *J. Phys. Chem. C* **2019**, *123*, 7431−7439.
(74) Zhao, Z.; Xu, H.; Feng, Z.; Zhang, Y.; Cui, M.; Cao, D.; Cheng, D. Design of High-Performance Co-Based Alloy Nanocatalysts for the Oxygen Reduction Reaction. *Chem.—Eur. J.* **2020**, *26*, 4128−4135.

https://dx.doi.org/10.1021/acsomega.0c05838
ACS Omega 2021, 6, 4888−4898